IJMMM International Journal of Minerals, Metallurgy and Materials 矿物冶金与材料学报（英文版）

Efficient energy transfer from self-trapped excitons to Mn^{2+} dopants in $CsCdCl_3:Mn^{2+}$ perovskite nanocrystals

Anran Zhang, Xinquan Zhou, Ranran Gu, and Zhiguo Xia

Cite this article as:

Anran Zhang, Xinquan Zhou, Ranran Gu, and Zhiguo Xia, Efficient energy transfer from self-trapped excitons to Mn^{2+} dopants in $CsCdCl_3:Mn^{2+}$ perovskite nanocrystals, *Int. J. Miner. Metall. Mater.*, 31(2024), No. 6, pp. 1456-1461. https://doi.org/10.1007/s12613-024-2844-5

View the article online at SpringerLink or IJMMM Webpage.

Articles you may be interested in

Lalinda Palliyaguru, Ushan S. Kulathunga, Lakruwani I. Jayarathna, Champa D. Jayaweera, and Pradeep M. Jayaweera, A simple and novel synthetic route to prepare anatase TiO_2 nanopowders from natural ilmenite via the H_3PO_4/NH_3 process, *Int. J. Miner. Metall. Mater.*, 27(2020), No. 6, pp. 846-855. https://doi.org/10.1007/s12613-020-2030-3

Lin-ping Wu, Guang-ping Huang, Chao-shi Hu, and Wei Victor Liu, Effects of cellulose nanocrystals on the acid resistance of cementitious composites, *Int. J. Miner. Metall. Mater.*, 28(2021), No. 11, pp. 1745-1758. https://doi.org/10.1007/s12613-020-2087-z

Xiao-hui Li, Jue Kou, Ti-chang Sun, Shi-chao Wu, and Yong-qiang Zhao, Formation of calcium titanate in the carbothermic reduction of vanadium titanomagnetite concentrate by adding $CaCO_3$, *Int. J. Miner. Metall. Mater.*, 27(2020), No. 6, pp. 745-753. https://doi.org/10.1007/s12613-019-1903-9

Azhar Iqbal, Long Chen, Yong Chen, Yu-xian Gao, Fang Chen, and Dao-cong Li, Lithium-ion full cell with high energy density using nickel-rich $LiNi_{0.8}Co_{0.1}Mn_{0.1}O_2$ cathode and SiO-C composite anode, *Int. J. Miner. Metall. Mater.*, 25(2018), No. 12, pp. 1473-1481. https://doi.org/10.1007/s12613-018-1702-8

Renuprava Dalai, Siddhartha Das, and Karabi Das, Relationship between the microstructure and properties of thermomechanically processed Fe-17Mn and Fe-17Mn-3Al steels, *Int. J. Miner. Metall. Mater.*, 26(2019), No. 1, pp. 64-75. https://doi.org/10.1007/s12613-019-1710-3

Seyed Esmaiel Shakib, Ramin Raiszadeh, and Jalil Vahdati-Khaki, A Self-propagating high-temperature synthesis process for the fabrication of Fe(Cr)-Al_2O_3 nanocomposite, *Int. J. Miner. Metall. Mater.*, 26(2019), No. 6, pp. 775-786. https://doi.org/10.1007/s12613-019-1779-8

IJMMM WeChat

QQ author group

INTERNATIONAL JOURNAL OF
Minerals, Metallurgy and Materials

Volume 31, Number 6, June 2024
Page 1456

Research Article https://doi.org/10.1007/s12613-024-2844-5

Efficient energy transfer from self-trapped excitons to Mn^{2+} dopants in $CsCdCl_3:Mn^{2+}$ perovskite nanocrystals

*Anran Zhang*1), *Xinquan Zhou*1), *Ranran Gu*1), *and Zhiguo Xia*1,2),✉

1) State Key Laboratory of Luminescent Materials and Devices, Guangdong Provincial Key Laboratory of Fiber Laser Materials and Applied Techniques, School of Materials Science and Engineering, South China University of Technology, Guangzhou 510641, China
2) School of Physics and Optoelectronics, South China University of Technology, Guangzhou 510641, China

(Received: 21 November 2023; revised: 21 January 2024; accepted: 29 January 2024)

Abstract: Mn^{2+} doping has been adopted as an efficient approach to regulating the luminescence properties of halide perovskite nanocrystals (NCs). However, it is still difficult to understand the interplay of Mn^{2+} luminescence and the matrix self-trapped exciton (STE) emission therein. In this study, Mn^{2+}-doped $CsCdCl_3$ NCs are prepared by hot injection, in which $CsCdCl_3$ is selected because of its unique crystal structure suitable for STE emission. The blue emission at 441 nm of undoped $CsCdCl_3$ NCs originates from the defect states in the NCs. Mn^{2+} doping promotes lattice distortion of $CsCdCl_3$ and generates bright orange-red light emission at 656 nm. The energy transfer from the STEs of $CsCdCl_3$ to the excited levels of the Mn^{2+} ion is confirmed to be a significant factor in achieving efficient luminescence in $CsCdCl_3:Mn^{2+}$ NCs. This work highlights the crucial role of energy transfer from STEs to Mn^{2+} dopants in Mn^{2+}-doped halide NCs and lays the groundwork for modifying the luminescence of other metal halide perovskite NCs.

Keywords: perovskite nanocrystals; self-trapped excitons; luminescence; energy transfer

1. Introduction

Perovskite-type compounds have become known as multifaceted functional materials, and the luminescence of self-trapped excitons (STEs) in metal halide perovskites, as an example, has garnered increasing attention in light-emitting diodes [1], scintillators [2], and sensors [3] due to their advantages of high photoluminescence quantum yield (PLQY), broadband emission, large Stokes shift, and long fluorescence lifetime. Strong electron–phonon coupling and soft lattice play crucial roles in the generation of STEs [4]. In general, STE emission occurs in low-dimensional metal halides because polyhedral distortions are more likely to occur at low connectivity [5]. Smith *et al.* [6] were the first to report typical Pb-based low-dimensional hybrid metal halides with broadband STE emission from 400 to 800 nm. Morad *et al.* [7] reported the fascinating photoluminescence in zero-dimensional (0D) Sb-based hybrid halides. It is also noticed that all-inorganic 0D $Cs_3Cu_2I_5$ displayed efficient broadband STE emission [8], and the associated synthesis has been extended from microcrystals to nanocrystals (NCs) [9]. However, realizing STE emission in all-inorganic three-dimensional (3D) halides is challenging, except for the reported $Cs_2AgInCl_6$ NCs [1]. This is because octahedra are solidly connected via shared corners in 3D halides, which makes lattice distortion difficult [10]. Interestingly, the unique bonding of 3D $CsCdCl_3$ can induce lattice distortion, thus potentially achieving STE emission, as reported elsewhere [11–12].

Extensive research on Mn^{2+} ions as dopants in several different metal halide NCs can be found in the recent literature [13–14]. Octahedrally coordinated Mn^{2+} can exhibit long-lived orange-red emission, originating from the spin-forbidden d–d transition. Among various halide NCs, $CsPbCl_3$ NCs with a suitable band gap have become an ideal host for efficient energy transfer from excitons to Mn^{2+} ions [15–16]. $CsCdCl_3$ is structurally similar to $CsPbCl_3$, but the lattice of $CsCdCl_3$ is easier to distort. Substituting Cd^{2+} with Mn^{2+} can further promote the distortion of the $CsCdCl_3$ lattice and facilitate the generation of STEs [10]. In addition, Mn^{2+} doping can form energy transfer channels from the host STEs to Mn^{2+} ions, thus exhibiting efficient orange-red emission [17]. Hence, $CsCdCl_3$ NCs were selected as the host for Mn^{2+} doping to investigate STE emission and the role of STEs in Mn^{2+} luminescence modulation.

In this study, $CsCdCl_3$ NCs are prepared by a hot-injection method and further doped with Mn^{2+} to form $CsCdCl_3:Mn^{2+}$ NCs. $CsCdCl_3$ NCs exhibit blue emission, which is ascribed to the defect states of the NCs. Mn^{2+} doping promotes the generation of STEs in $CsCdCl_3$ NCs and forms energy transfer channels from STEs to the Mn^{2+} ion, giving rise to bright orange-red emission in $CsCdCl_3:Mn^{2+}$ NCs. This work provides alternative strategies for STE emission research in 3D metal halide NCs and optimization of

---

✉ Corresponding author: Zhiguo Xia E-mail: xiazg@scut.edu.cn

Springer

their luminescence performance.

2. Experimental

2.1. Materials

Cesium carbonate (Cs_2CO_3, 99.9wt%), manganese acetate tetrahydrate ($Mn(CH_3COO)_2·4H_2O$, analytical pure), oleic acid (OA, analytical pure), oleylamine (OLA, 80wt%–90wt%), octadecene (ODE, >90wt%), benzoyl chloride (BzCl, 98wt%), *n*-hexane (C_6H_{14}, ≥98wt%), and ethyl acetate ($C_4H_8O_2$, analytical pure) were purchased from Aladdin. Cadmium acetate dihydrate ($Cd(CH_3COO)_2·2H_2O$, analytical pure) was purchased from Macklin. All chemicals were used without further purification.

2.2. Synthesis

Cs_2CO_3 (0.125 mmol), $Cd(CH_3COO)_2·2H_2O$ (0.25 mmol), $Mn(CH_3COO)_2·4H_2O$ (0.05 mmol in general experiments, i.e., the Mn/Cd precursor ratio was 20%. For $CsCd_{1-x}Cl_3$:$x$$Mn^{2+}$ NCs, x = 0.05, 0.10, 0.15, 0.20, and 0.25, and the total amount of $Cd(CH_3COO)_2·2H_2O$ and $Mn(CH_3COO)_2·4H_2O$ was 0.25 mmol.), OLA (2 mL), OA (2 mL), and ODE (8 mL) were placed in a 50 mL three-neck flask. The mixed solution was heated to 120°C and degassed by alternating vacuum and N_2 for 30 min. Afterward, the mixture was heated to 200°C under N_2. Then, 0.4 mL of BzCl was swiftly injected into the flask under vigorous stirring. The reaction was quenched in an ice-water bath after 10 s. The crude solution was centrifuged at 8000 r/min for 5 min. The precipitate fraction was redispersed in 10 mL of *n*-hexane and centrifuged at 4000 r/min for 3 min, leaving the supernatant. After that, the NCs were precipitated with 30 mL of ethyl acetate by centrifugating at 8000 r/min for 5 min. Finally, half of the precipitate was dispersed in *n*-hexane and the other half was dried in an oven to make into powder for the following use.

2.3. Characterization

X-ray diffraction (XRD) was conducted using an Aeris XRD instrument (PANalytical, Netherlands) at 40 kV and 15 mA with monochromatized Cu K_α radiation (λ = 1.5406 Å) and linear VANTEC detector. The samples were prepared by dissolving the NCs in *n*-hexane and dropping the concentrated solutions onto a silicon substrate. Transmission electron microscopy (TEM), high-resolution TEM (HRTEM), and energy-dispersive X-ray spectroscopy (EDS) were performed using a JEM-2010 instrument at 120 kV and equipped with an energy-dispersive detector. The samples for TEM analysis were prepared by dropping dilute NC solutions onto 300 mesh copper grids coated with ultrathin carbon film. Room-temperature photoluminescence excitation (PLE), photoluminescence (PL), and time-resolved PL (TRPL) spectra were collected using an FLS1000 fluorescence spectrophotometer (Edinburgh Instruments Ltd., U.K.). Temperature-dependent spectra were recorded on the same spectrophotometer equipped with the cryogenic liquid nitrogen plant equipment. PLQYs were determined via an absolute PL quantum yield spectrometer (Quantaurus-QY Plus C13534-11, Hamamatsu Photonics). All optical measurements were conducted on NC powders in ambient conditions.

3. Results and discussion

3.1. Structure and synthesis

Perovskite-type $CsCdCl_3$ crystallizes into a hexagonal structure (space group $P6_3/mmc$) with $[Cd_2Cl_9]^{5-}$ subunits sharing corners with $[CdCl_6]^{4-}$ octahedra (Fig. 1(a)). The distinct symmetries of Cd endow the structure with two types of symmetry, D_{3d} and C_{3v} [12,18]. The dopant Mn^{2+} ions are supposed to substitute the octahedral Cd^{2+} sites. As illustrated in Fig. 1(b), Mn^{2+}-doped $CsCdCl_3$ NCs are synthesized via a modified hot-injection method [19]. As described in the Experimental Section, precursors (Cs carbonate and Cd, Mn acetates) are dissolved in ODE with OA and OLA. When the system is heated to 200°C, rapid injection of BzCl can trigger the nucleation and growth of the NCs. The Mn^{2+} doping concentration in $CsCdCl_3$:Mn^{2+} NCs is 20% (molar ratio of the precursor), and all analyses are based on the samples with this concentration. The XRD pattern demonstrates pure-phase NCs (not easy to form impurities like Cs_2CdCl_4 and $Cs_3Cd_2Cl_7$) (Fig. 1(c)). After Mn^{2+} doping, the diffraction peak at 23.98° shifts slightly toward higher angles, which can be ascribed to lattice contraction induced by the substitution of Cd^{2+} (Radius, r = 0.95 Å; coordination number, CN = 6)

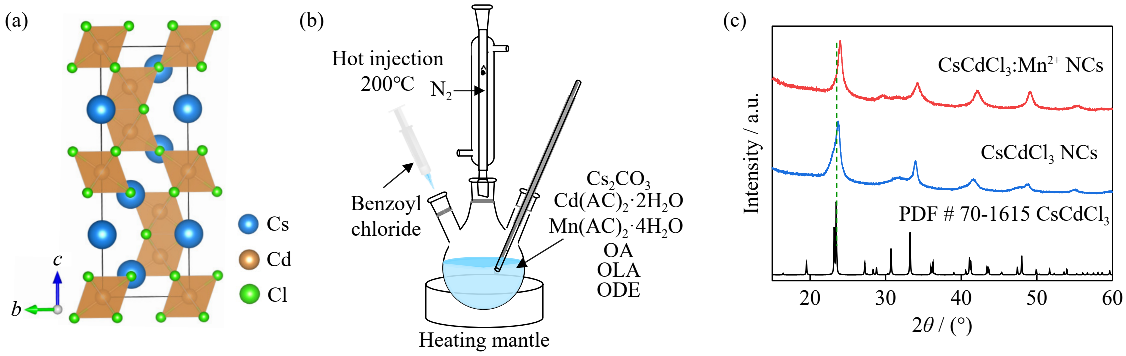

Fig. 1. (a) Crystal structure diagram of $CsCdCl_3$. (b) Synthesis illustration of $CsCdCl_3$:Mn^{2+} NCs. (c) XRD patterns of $CsCdCl_3$ and $CsCdCl_3$:Mn^{2+} NCs.

with smaller Mn^{2+} (r = 0.83 Å, CN = 6), showing the successful doping of Mn^{2+} in the $CsCdCl_3$ lattice.

3.2. TEM analysis

In the TEM images, $CsCdCl_3$ and $CsCdCl_3:Mn^{2+}$ NCs present distorted square-like morphologies with similar mean sizes of (10.1 ± 1.5) and (10.8 ± 1.8) nm, respectively (Fig. 2(a) and (b)). The HRTEM images in Fig. 2(c) and (d) clearly show the lattice fringes of the NCs, verifying their high crystallinity. The interplanar spacings (3.66 and 3.63 Å) correspond to the (110) planes. Further EDS elemental mapping of $CsCdCl_3:Mn^{2+}$ NCs reveals the homogeneous distribution of Cs, Cd, Cl, and Mn in the NCs (Fig. 2(e)).

3.3. PL spectra analysis

The optical properties of undoped $CsCdCl_3$ and Mn^{2+}-doped $CsCdCl_3$ NCs were studied as a comparison. In Fig. 3(a), when excited at 365 nm (λ_{ex}), $CsCdCl_3$ NCs display blue emission at 441 nm (λ_{em}) with a PLQY of 8.6%. Given the asymmetric emission band and the fact that no such blue emission has been observed in reported $CsCdCl_3$ crystals [20–21], we propose the emission is not inherent to $CsCdCl_3$. The decay behavior of the 441 nm emission can be well fitted by a single exponential function with a short lifetime (τ) of 5.78 ns. Based on these results, the blue emission can be assigned to the defect states or surface states of $CsCdCl_3$ NCs [22–24]. Besides the above blue emission, when excited at 265 nm, $CsCdCl_3:Mn^{2+}$ NCs display orange-red emission at 656 nm with full width at half-maximum (FWHM) of 113 nm and PLQY of 11.1% (Fig. 3(b)). Combined with the excitation spectrum, the main peak of this emission can be attributed to the Mn^{2+} d–d transition ($^4T_1 \rightarrow {}^6A_1$) [25]. It is noted that this orange-red emission peak has a relatively large FWHM and imperfect symmetry, implying the possible presence of additional emission centers. In Fig. 3(c) below, the decay curve of the emission can be well fitted by a biexponential function with a short lifetime of 0.24 ms and a long lifetime of 0.94 ms. The fast decay indicates STE emission resulting from lattice distortion after Mn^{2+} doping, which will be discussed in detail later. The slow component indicates the spin-forbidden transition of Mn^{2+} ($^4T_1 \rightarrow {}^6A_1$), as found in other

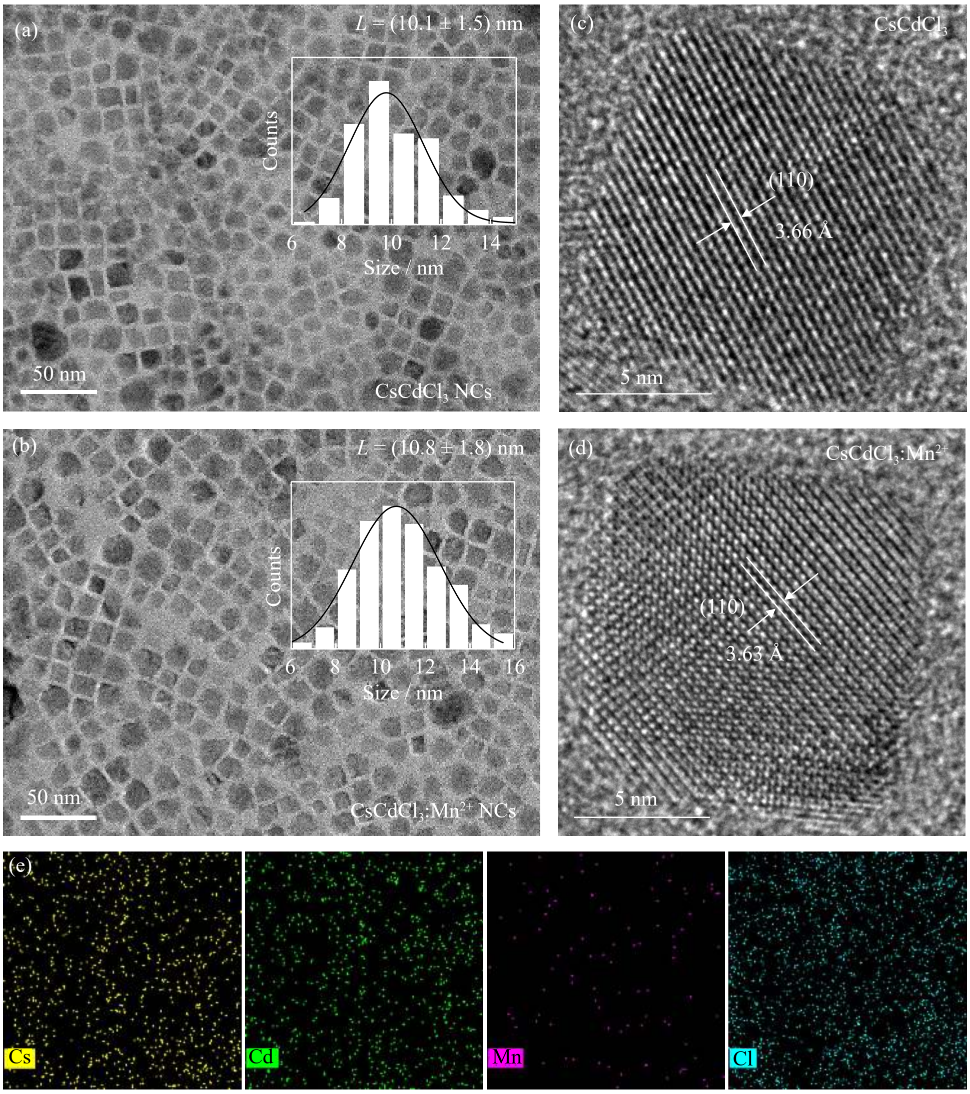

Fig. 2. (a, b) TEM images and size distribution histograms (inset) of $CsCdCl_3$ and $CsCdCl_3:Mn^{2+}$ NCs. (c, d) HRTEM images of $CsCdCl_3$ and $CsCdCl_3:Mn^{2+}$ NCs. (e) EDS elemental mapping (Cs, Cd, Cl, and Mn) of $CsCdCl_3:Mn^{2+}$ NCs.

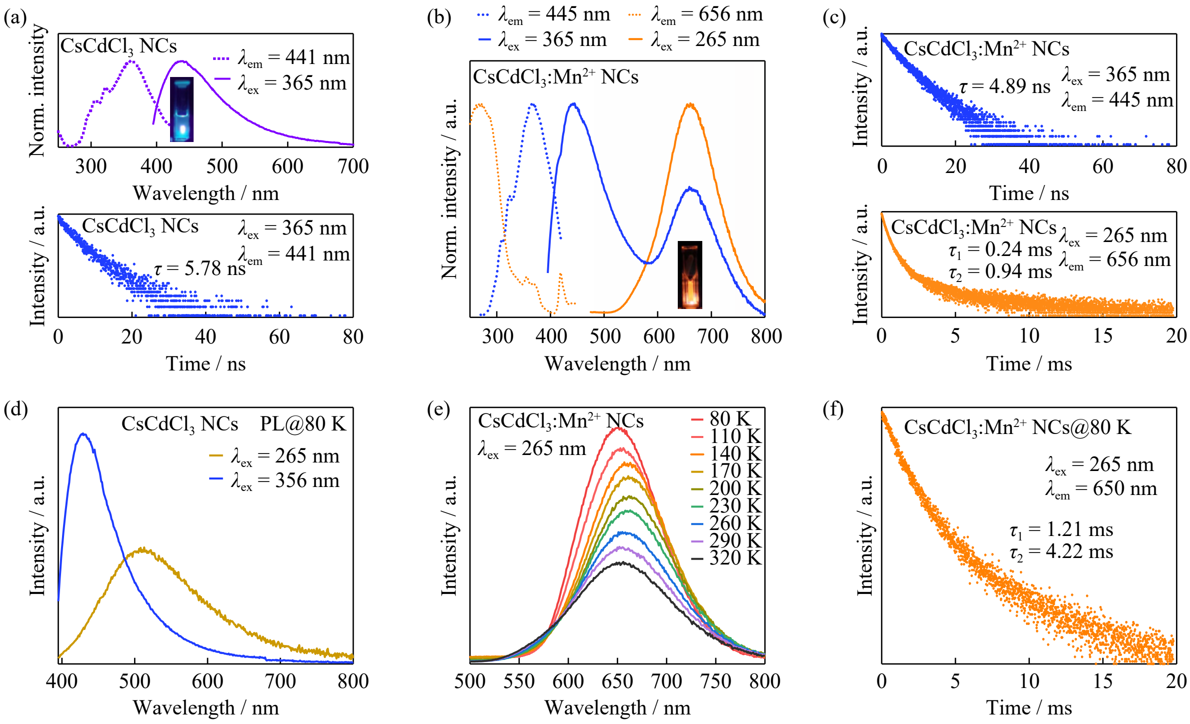

Fig. 3. (a) PLE, PL, and TRPL spectra of $CsCdCl_3$ NCs. (b) PLE and PL spectra of $CsCdCl_3$:Mn^{2+} NCs under different emission and excitation wavelengths. (c) TRPL spectra of $CsCdCl_3$:Mn^{2+} NCs at 445 nm (upper) and 656 nm (under). (d) PL spectra of $CsCdCl_3$ NCs at 80 K (λ_{ex} = 265 and 365 nm). (e) Temperature-dependent PL spectra of $CsCdCl_3$:Mn^{2+} NCs (λ_{ex} = 265 nm). (f) TRPL spectrum of $CsCdCl_3$:Mn^{2+} NCs at 80 K.

systems [26–27].

To further elucidate the luminescence mechanism of $CsCdCl_3$:Mn^{2+} NCs, temperature-dependent steady-state and transient-state PL spectra were recorded and compared. $CsCdCl_3$ NCs exhibit blue emission at 80 K when excited at 365 nm, which arises from the previously discussed defect states or surface states of NCs. Notably, under 265 nm excitation at 80 K, $CsCdCl_3$ NCs show broadband emission (FWHM = 155 nm) in the 400–700 nm range, which agrees with the attributes of STE emission (Fig. 3(d)). As stated above, the octahedron with C_{3v} symmetry is slightly distorted, leading to STE emission [10,28]. The emission in the NCs is not as pronounced as that in the crystals at room temperature [29] but can be easily observed at low temperatures [30]. Mn^{2+} doping further promotes $CsCdCl_3$ lattice distortion, allowing the observation of STE emission from low to room temperature. In Fig. 3(e), the PL peak is asymmetric, with a tail in the 500–600 nm range. Moreover, the improved PL intensity and prolonged PL lifetime with decreasing temperature can be ascirbed to suppressed nonradiative relaxation (Fig. 3(e) and (f)).

The PLE spectra of $CsCd_{1-x}Cl_3$:xMn^{2+} NCs (x = 0.05, 0.10, 0.15, 0.20, and 0.25) under various optimum emission wavelengths are displayed in Fig. 4(a). The excitation peaks in the 250–270 nm range are associated with the charge transfer band (CTB) of $Cl^- \rightarrow Mn^{2+}$. The narrow excitation bands in the 330–450 nm range are assigned to the d–d transitions of the Mn^{2+} ion. Specifically, the peaks at 330, 360, 380, and 420 nm correspond to the $^6A_1 \rightarrow {}^4T_1(^4P)$, $^6A_1 \rightarrow {}^4E(^4D)$, $^6A_1 \rightarrow {}^4T_2(^4D)$, and $^6A_1 \rightarrow {}^4A_1(^4G)/{}^4E(^4G)$ transitions of the Mn^{2+} ion, respectively [29]. With increasing Mn^{2+} concentration, the CTB shows a slight blue shift, and the intensity of Mn^{2+}-related excitation peaks increases. As depicted in Fig. 4(b), the PL spectra of $CsCd_{1-x}Cl_3$:xMn^{2+} NCs with increasing Mn^{2+} concentration show that the STE emission is gradually weakened, and the emission mainly manifests as the characteristic emission of Mn^{2+} ions. On the other hand, the emission peaks display a red shift from 650 to 667 nm with narrow FWHMs. Given that both STE and Mn^{2+} emissions are excited at 265 nm, the bright orange-red emission of the Mn^{2+}-doped NCs most likely originates from an efficient energy transfer from STEs to the energy levels of the Mn^{2+} ion, which is consistent with other studies [10,12,31]. Notably, the STE emission band is more easily observed at low doping concentrations. In Fig. 4(c), two Gaussian peaks can be well fitted to the spectral profile. The 577 nm peak can be assigned to STE emission, while the 657 nm peak can be assigned to Mn^{2+} d–d transition. These results imply that there are two luminescence mechanisms in $CsCdCl_3$:Mn^{2+} NCs, as illustrated in Fig. 4(d). Excitons under 265 nm excitation are trapped by shallow defects proximal to the conduction band. These excitons, due to thermal perturbations, can be rereleased and subsequently undergo recombination (STE emission at 577 nm) or be captured by Mn^{2+} dopants. The captured excitons will relax to the lowest excited state ($^4T_1$) and then undergo the radiative transition from $^4T_1$ to $^6A_1$, resulting in bright orange-red emission at 657 nm. In the process, Mn^{2+} doping promotes $CsCdCl_3$ lattice distortion and the generation of STEs. The energy transfer from STEs to Mn^{2+} enables efficient luminescence of Mn^{2+} ions and large

Stokes shift.

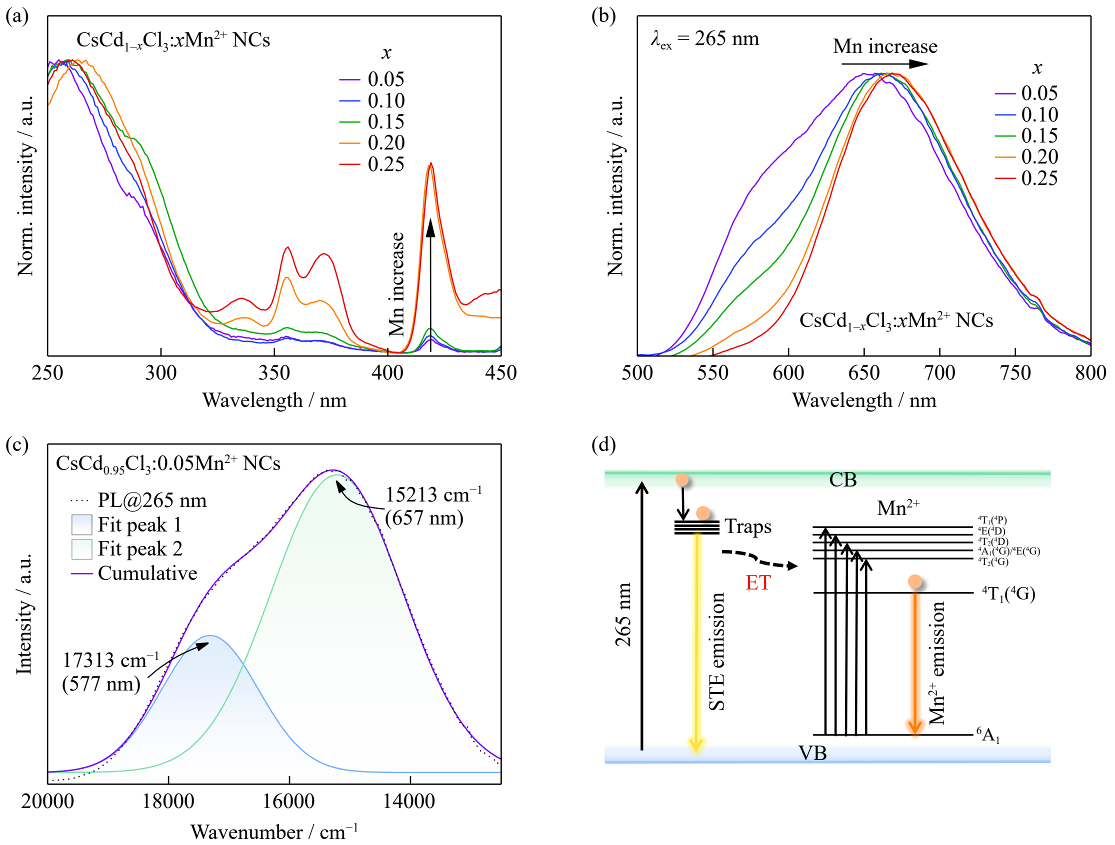

Fig. 4. (a) PLE (λ_{em} = 650, 657, 659, 663, and 667 nm) and (b) PL spectra (λ_{ex} = 265 nm) of $CsCd_{1-x}Cl_3:xMn^{2+}$ NCs with different Mn^{2+} concentrations (x = 0.05, 0.10, 0.15, 0.20, and 0.25). (c) PL spectra and Gaussian fitting curves of $CsCd_{0.95}Cl_3:0.05Mn^{2+}$ NCs excited at 265 nm. (d) Schematic of the energy transfer mechanism from STEs to Mn^{2+} d–d transition in the $CsCdCl_3:Mn^{2+}$ NCs (CB: conduction band; VB: valence band; ET: energy transfer).

4. Conclusion

In summary, $CsCdCl_3:Mn^{2+}$ NCs are successfully synthesized via a hot-injection method. The blue emission at 441 nm of undoped $CsCdCl_3$ NCs can be assigned to the defect states of the NCs. Mn^{2+} doping further promotes $CsCdCl_3$ lattice distortion, facilitating the generation of STEs. Mn^{2+}-doped $CsCdCl_3$ NCs display bright orange-red emission at 656 nm. The obtained results revealed that the energy transfer from the STEs of $CsCdCl_3$ to the energy levels of the Mn^{2+} ion is a significant factor in realizing efficient luminescence in $CsCdCl_3:Mn^{2+}$ NCs. This work extends the research on STE emission in 3D metal halide NCs and provides useful approaches to improving the luminescence performance of metal halide NCs.

Acknowledgements

This work was supported by the Guangdong Provincial Science & Technology Project (No. 2023A0505050084), the National Natural Science Foundation of China (No. 22361132525), the Fundamental Research Funds for the Central Universities (No. 2023ZYGXZR002), and the Local Innovative and Research Teams Project of Guangdong Pearl River Talents Program (No. 2017BT01X137).

Conflict of Interest

Zhiguo Xia is an editorial board member for this journal and was not involved in the editorial review or the decision to publish this article. The authors declare no potential conflict of interest.

References

[1] W.B. Chen, W. Li, X.J. Zhang, *et al.*, Carbon dots embedded in lead-free luminescent metal halides crystals towards single-component white emitters, *Sci. China Mater.*, 65(2022), No. 10, p. 2802.

[2] W.J. Zhu, W.B. Ma, Y.R. Su, *et al.*, Low-dose real-time X-ray imaging with nontoxic double perovskite scintillators, *Light Sci. Appl.*, 9(2020), art. No. 112.

[3] M.Z. Li and Z.G. Xia, Recent progress of zero-dimensional luminescent metal halides, *Chem. Soc. Rev.*, 50(2021), No. 4, p. 2626.

[4] Y.Y. Jing, Y. Liu, M.Z. Li, and Z.G. Xia, Photoluminescence of singlet/triplet self-trapped excitons in Sb^{3+}-based metal halides, *Adv. Opt. Mater.*, 9(2021), No. 8, art. No. 2002213.

[5] C.K. Deng, G.J. Zhou, D. Chen, J. Zhao, Y.G. Wang, and Q.L. Liu, Broadband photoluminescence in 2D organic–inorganic hybrid perovskites: $(C_7H_{18}N_2)PbBr_4$ and $(C_9H_{22}N_2)PbBr_4$, *J. Phys. Chem. Lett.*, 11(2020), No. 8, p. 2934.

[6] M.D. Smith, B.L. Watson, R.H. Dauskardt, and H.I. Karunadasa, Broadband emission with a massive stokes shift from

sulfonium Pb–Br hybrids, *Chem. Mater.*, 29(2017), No. 17, p. 7083.

[7] V. Morad, S. Yakunin, B.M. Benin, *et al.*, Hybrid 0D antimony halides as air-stable luminophores for high-spatial-resolution remote thermography, *Adv. Mater.*, 33(2021), No. 9, art. No. 2007355.

[8] T. Jun, K. Sim, S. Iimura, *et al.*, Lead-free highly efficient blue-emitting $Cs_3Cu_2I_5$ with 0D electronic structure, *Adv. Mater.*, 30(2018), No. 43, art. No. 1804547.

[9] L.Y. Lian, M.Y. Zheng, W.Z. Zhang, *et al.*, Efficient and reabsorption-free radioluminescence in $Cs_3Cu_2I_5$ nanocrystals with self-trapped excitons, *Adv. Sci.*, 7(2020), No. 11, art. No. 2000195.

[10] J.H. Han, T. Samanta, Y.M. Park, *et al.*, Effect of self-trapped excitons in the optical properties of manganese-alloyed hexagonal-phased metal halide perovskite, *Chem. Eng. J.*, 450(2022), art. No. 138325.

[11] W.Y. Jia, Q.L. Wei, S.F. Yao, *et al.*, Magnetic coupling for highly efficient and tunable emission in $CsCdX_3$:Mn perovskites, *J. Lumin.*, 257(2023), art. No. 119657.

[12] Z. Tang, R.Z. Liu, J.S. Chen, *et al.*, Highly efficient and ultralong afterglow emission with anti-thermal quenching from $CsCdCl_3$:Mn perovskite single crystals, *Angew. Chem. Int. Ed.*, 61(2022), No. 51, art. No. e202210975.

[13] B.B. Su, G.J. Zhou, J.L. Huang, E.H. Song, A. Nag, and Z.G. Xia, Mn^{2+}-doped metal halide perovskites: Structure, photoluminescence, and application, *Laser Photonics Rev.*, 15(2021), No. 1, art. No. 2000334.

[14] F. Locardi, M. Cirignano, D. Baranov, *et al.*, Colloidal synthesis of double perovskite $Cs_2AgInCl_6$ and Mn-doped $Cs_2AgInCl_6$ nanocrystals, *J. Am. Chem. Soc.*, 140(2018), No. 40, p. 12989.

[15] S.D. Adhikari, A. Dutta, S.K. Dutta, and N. Pradhan, Layered perovskites $L_2(Pb_{1-x}Mn_x)Cl_4$ to Mn-doped $CsPbCl_3$ perovskite platelets, *ACS Energy Lett.*, 3(2018), No. 6, p. 1247.

[16] X. Yuan, S.H. Ji, M.C.D. Siena, *et al.*, Photoluminescence temperature dependence, dynamics, and quantum efficiencies in Mn^{2+}-doped $CsPbCl_3$ perovskite nanocrystals with varied dopant concentration, *Chem. Mater.*, 29(2017), No. 18, p. 8003.

[17] K.Y. Xu and A. Meijerink, Tuning exciton–Mn^{2+} energy transfer in mixed halide perovskite nanocrystals, *Chem. Mater.*, 30(2018), No. 15, p. 5346.

[18] X.Q. Zhou, K. Han, Y.X. Wang, *et al.*, Energy-trapping management in X-ray storage phosphors for flexible 3D imaging, *Adv. Mater.*, 35(2023), No. 16, art. No. 2212022.

[19] A.R. Zhang, Y. Liu, G.C. Liu, and Z.G. Xia, Dopant and compositional modulation triggered broadband and tunable near-infrared emission in $Cs_2Ag_{1-x}Na_xInCl_6$:Cr^{3+} nanocrystals, *Chem. Mater.*, 34(2022), No. 7, p. 3006.

[20] R. Demirbilek, A.Ç. Bozdoğan, M. Çalışkan, G. Asan, and G. Özen, Electronic energy levels of $CsCdCl_3$, *J. Lumin.*, 131(2011), No. 9, p. 1853.

[21] Y. Zhang, L. Zhou, D. Li, *et al.*, Realizing efficient emission in three-dimensional $CsCdCl_3$ single crystals by introducing separated emitting centers, *Inorg. Chem.*, 61(2022), No. 44, p. 17902.

[22] M.Y. Leng, Y. Yang, Z.W. Chen, *et al.*, Surface passivation of bismuth-based perovskite variant quantum dots to achieve efficient blue emission, *Nano Lett.*, 18(2018), No. 9, p. 6076.

[23] Y.Y. Jing, Y. Liu, J. Zhao, and Z.G. Xia, Sb^{3+} doping-induced triplet self-trapped excitons emission in lead-free Cs_2SnCl_6 nanocrystals, *J. Phys. Chem. Lett.*, 10(2019), No. 23, p. 7439.

[24] Y. Liu, Y.Y. Jing, J. Zhao, Q.L. Liu, and Z.G. Xia, Design optimization of lead-free perovskite $Cs_2AgInCl_6$:Bi nanocrystals with 11.4% photoluminescence quantum yield, *Chem. Mater.*, 31(2019), No. 9, p. 3333.

[25] Y.X. Huang, Y.X. Pan, S.T. Guo, C.D. Peng, H.Z. Lian, and J. Lin, Large spectral shift of Mn^{2+} emission due to the shrinkage of the crystalline host lattice of the hexagonal $CsCdCl_3$ crystals and phase transition, *Inorg. Chem.*, 61(2022), No. 21, p. 8356.

[26] W. Zhang, J.J. Wei, Z.L. Gong, *et al.*, Unveiling the excited-state dynamics of Mn^{2+} in 0D Cs_4PbCl_6 perovskite nanocrystals, *Adv. Sci.*, 7(2020), No. 22, art. No. 2002210.

[27] P. Arunkumar, K.H. Gil, S. Won, *et al.*, Colloidal organolead halide perovskite with a high Mn solubility limit: A step toward Pb-free luminescent quantum dots, *J. Phys. Chem. Lett.*, 8(2017), No. 17, p. 4161.

[28] R. Yang, D. Yang, M. Wang, *et al.*, High-efficiency and stable long-persistent luminescence from undoped cesium cadmium chlorine crystals induced by intrinsic point defects, *Adv. Sci.*, 10(2023), No. 15, art. No. 2207331.

[29] S.S. He, Q.P. Qiang, T.C. Lang, *et al.*, Highly stable orange-red long-persistent luminescent $CsCdCl_3$:Mn^{2+} perovskite crystal, *Angew. Chem. Int. Ed.*, 61(2022), No. 48, art. No. e202208937.

[30] S.G. Ge, H. Peng, Q.L. Wei, *et al.*, Realizing color-tunable and time-dependent ultralong afterglow emission in antimony-doped $CsCdCl_3$ metal halide for advanced anti-counterfeiting and information encryption, *Adv. Opt. Mater.*, 11(2023), No. 14, art. No. 2300323.

[31] W.X. Dong, Y.C. Xu, P. Su, *et al.*, Excitation wavelength-dependent long-afterglow Sb, Mn-doped $CsCdCl_3$ perovskite for anti-counterfeiting applications, *Ceram. Int.*, 50(2024), No. 4, p. 6374.